

Article

Structural Reliability of Plain Bearings for Wave Energy Converter Applications

Simon Ambühl ^{1,*}, Morten Kramer ^{1,2} and John Dalsgaard Sørensen ¹

¹ Department of Civil Engineering, Aalborg University, Sofiendalsvej 11, Aalborg SV 9200, Denmark; mmk@civil.aau.dk (M.K.); jds@civil.aau.dk (J.D.S.)

² Wave Star A/S, Park Allé, Brøndby 2605, Denmark

* Correspondence: sia@civil.aau.dk; Tel.: +45-9940-8565; Fax: +45-9940-8552

Academic Editor: John Ringwood

Received: 4 December 2015; Accepted: 4 February 2016; Published: 19 February 2016

Abstract: The levelized cost of energy (LCOE) from wave energy converters (WECs) needs to be decreased in order to be able to become competitive with other renewable electricity sources. Probabilistic reliability methods can be used to optimize the structure of WECs. Optimization is often performed for critical structural components, like welded details, bolts or bearings. This paper considers reliability studies with a focus on plain bearings available from stock for the Wavestar device, which exists at the prototype level. The Wavestar device is a point absorber WEC. The plan is to mount a new power take-off (PTO) system consisting of a discrete displacement cylinder (DDC), which will allow different hydraulic cycles to operate at constant pressure levels. This setup increases the conversion efficiency, as well as decouples the electricity production from the pressure variations within the hydraulic cycle when waves are passing. The new PTO system leads to different load characteristics at the floater itself compared to the actual setup where the turbine/generator is directly coupled to the fluctuating hydraulic pressure within the PTO system. This paper calculates the structural reliability of the different available plain bearings planned to be mounted at the new PTO system based on a probabilistic approach, and the paper gives suggestions for fulfilling the minimal target reliability levels. The considered failure mode in this paper is the brittle fatigue failure of plain bearings. The performed sensitivity analysis shows that parameters defining the initial crack size have a big impact on the resulting reliability of the plain bearing.

Keywords: plain bearing; probabilistic reliability assessment; sensitivity analysis; structural reliability; wave energy converter; Wavestar

1. Introduction

Wave energy converters (WECs) are used to harvest energy from waves and transfer that to electricity. So far, many different working principles exist; some of them have reached the prototype level, while others exist at the lab scale or just on paper, but none have reached a developed stage where electricity can be produced at a competitive level. In order to drive the development, the levelized cost of energy (LCOE) needs to be decreased to become competitive with other renewable electricity sources. One way to decrease the cost of electricity produced by WECs is based on developing structural standards for the WEC community in order to standardize the structural designs, as well as giving guidelines to the WEC developers. Standards can also be used as a collection of gained knowledge. The challenge concerning standardization of WEC structures is the large diversity of different WECs. The work in [1,2] shows and explains the development stage of many different existing devices.

The past showed that standards should be developed for WECs especially for critical structural details, which in the case of failure will lead to large consequences. An example of WEC failure

due to structural failures is the broken force transducer connecting the anchoring block and the main mooring line of the wave dragon device during a storm [3]. The device was stranded at the beach. Other examples of structural failure of WECs is the prototype Osprey1, which failed structurally shortly after deployment in 1995 due to damage that happened during launching the device [4] or failure of the composite hull structure of one of Wavestar's floaters during a storm in June 2010 [5].

For WEC applications, critical structural details include welded details, bolts, as well as bearings. These structural components interconnect two structural parts and will lead in the case of failure to a partial or total collapse of the overall structure. In order to appropriate these critical structural components, detailed structural reliability investigations are needed.

Detailed structural reliability studies are commonly based on a probabilistic approach that considers the uncertainties related to limited knowledge, the physical variation of parameters, the models used to calculate stresses and loads, as well as the limited size of available data and the measurement uncertainties resulting from experiments and tests. There have been structural reliability studies on bolted and welded details previously with a focus on WEC applications (see, e.g., [6,7]). Bearings are also of importance for WEC applications, but so far, there has not been any reliability studies on bearings for WEC applications based on a probabilistic reliability approach. Bearing components for WEC applications may be custom-made, which will lead to a higher risk of failure due to limited knowledge and experience. Furthermore, WEC systems include a control system, which influences the loads on the bearings. Load impacts by the control system should be accounted for when doing probabilistic reliability assessments of bearings. WEC bearings are exposed to cyclic loading with frequencies in the range of the passing waves.

Reliability studies of bearings used in other offshore industry branches, like the oil and gas sector or offshore wind turbines, cannot be adopted due to the fact that the load characteristics, as well as the rotational speed ranges are different for the several offshore technologies. When comparing reliability levels for different applications, another fact for consideration is the different consequences in the case of failure leading to different target reliability levels. Structural collapse of a manned oil platform will lead to large environmental pollution and fatalities, whereas WECs are unmanned most of the time, and structural failure will lead to low environmental pollution. For WEC applications, the maximum annual probabilities of failure of structural components are typically accepted to be in the range between 10^{-4} and 10^{-3} [6]. This maximum annual probability of structural failure is adopted from offshore wind turbine applications (see, e.g., [8]) due to the fact that the consequences, such as low environmental pollution or no danger of fatalities in the case of structural failure, are the same for offshore wind turbines and WECs. The same reliability levels are also considered for tidal turbines; see, e.g., the recently published standard [9].

For WECs with many moving parts and a structure exposed to cyclic loading due to the waves and the wind, fatigue failure is of importance. Furthermore, many devices have a so-called "storm protection mode" or "idle mode", where the loads on the structure are decreased during storms. This means that extreme loads might not occur during storm events, but during operation.

This paper presents a case study with a focus on the fatigue failure of steel plain bearings. The bearing connecting the power take-off (PTO) and the floater arm of the Wavestar device, which is placed at Hanstholm on the Danish West coast of the North Sea, is considered as a case study. Simulated load time series are used as input for the probabilistic reliability assessment. More information about the considered PTO system of the Wavestar device is available in [10]. More information about the Wavestar device in general is available, e.g., in [5,11]. A parametric study is performed in order to assess the sensitivity of the different considered parameters, as well as the reliability level of different plain bearings available from stock.

Sections 2 and 3 respectively give the theoretical background about the probabilistic reliability assessments and failure modes of bearings. Section 4 explains in more detail the Wavestar device, which is considered as a case study in this article. Section 5 presents the considered fatigue model for

modeling bearing failure. Section 6 shows the resulting annual reliability values of the study, as well as a sensitivity study on uncertain parameters, and Section 7 gives the conclusion of the results.

2. Probabilistic Reliability Assessments

Probabilistic reliability assessments can be formulated for a certain failure mode or system of failure modes. The physical background of the failure mode needs to be known to be able to formulate a limit-state equation. Probabilistic reliability assessments consider uncertainties. The following uncertainty types can be included in probabilistic reliability assessments:

- Physical uncertainties,
- Modeling uncertainties,
- Statistical uncertainties,
- Measurement uncertainties.

Physical uncertainties consider uncertainties that cannot be reduced and are always present. Examples of physical uncertainties are the inter-annual variation of extreme significant wave heights, as well as yield stress differences when performing tensile tests. Physical uncertainties are also called aleatory uncertainties. Modeling uncertainties account for uncertainties related to the considered load/stress models and resistance models. Statistical uncertainties are of importance where small datasets are used, and this uncertainty type accounts for the limited dataset. When measurements are used in order to estimate the resistance or the load, there will be measurement uncertainties.

Uncertain parameters and uncertainties in general are treated as stochastic variables in probabilistic reliability assessments. Stochastic variables have a certain mean value and a certain standard deviation. The stochastic variables are summarized in a vector called $\mathbf{X} = [X_1, X_2, \dots]$. For a certain failure mode, a limit state equation, $g(\mathbf{X}, t)$, consisting of the resistance $R(\mathbf{X}, t)$ and the load $S(\mathbf{X}, t)$, can be established as a function of time t , if relevant, as is the case for fatigue failures:

$$g(\mathbf{X}, t) = R(\mathbf{X}, t) - S(\mathbf{X}, t) \quad (1)$$

From the limit state equation, based on Monte Carlo simulations or FORM/SORM (first/second order reliability methods) techniques, the probability of failure, P_F , can be estimated for a certain failure mode. This probability of failure is equal to the probability that the limit state equation (see Equation (1)) is smaller than or equal to zero. More information about probabilistic reliability methods for structural details is available in, e.g., [12,13]. From the FORM/SORM techniques, the so-called reliability index, $\beta(\mathbf{X}, t)$, is determined and can be used to estimate the probability of failure in the time interval $[0, t]$:

$$P_F(\mathbf{X}, t) = P_F(g(\mathbf{X}, t) \leq 0) = \Phi(-\beta(\mathbf{X}, t)) \quad (2)$$

where $\Phi()$ is the standardized normal distribution. The time interval, for which the reliability is estimated, is often assumed to be one year. The annual probability of failure, $\Delta P_F(\mathbf{X}, t)$, can be estimated from the cumulative probability of failure ($P_F(\mathbf{X}, t)$) at a certain time t :

$$\Delta P_F(\mathbf{X}, t) = P_F(t) - P_F(t - T) \quad (3)$$

where $T = 1$ year and $t > T$. Table 1 shows the relation between the probability of failure P_F and the resulting reliability index β . When performing reliability assessments, target reliability levels leading to acceptable minimal reliability indices or maximal probability failures should be defined in order to accept or reject a certain design. The target reliability levels mainly depend on the consequences in the case of failure. For WEC applications, the consequences in the case of structural failure are mainly of monetary value. The work in [14] proposes minimal annual probabilities of failure for ultimate limit states in the range between 10^{-3} and 10^{-4} , which is equal to a minimal annual reliability index, $\Delta\beta$, of 3.1 and 3.7, for cases where the relative cost of safety measure is large and the objective is to minimize the overall costs. This target minimal reliability index range is also used in [6], where

structural safety factors for welded and bolted WEC structures are calibrated. The same annual maximal probability of the failure range is used for offshore wind turbines (see, e.g., [8]).

Table 1. Relation between the probability of failure P_F and the resulting reliability index β .

P_F	10^{-6}	10^{-5}	10^{-4}	10^{-3}	10^{-2}
β	4.7	4.3	3.7	3.1	2.3

3. Failure Modes of Bearings

Bearings are connection elements of two structural parts where it is necessary that these two structural components can move with respect to each other. There are so-called contact bearings where mechanical contact exists between two components, as well as non-contact bearings. Non-contact bearings include magnetic bearings, externally pressurized, as well as hydrodynamic fluid-film bearings. The motion of the bearing can be linear or rotational, dependent on the application and bearing type.

For WEC applications, it is expected that mainly contact bearings will be used due to their simple construction with a low amount of elements and no need for additional energy sources. Many non-contact bearings need a power source in order to operate. Furthermore, offshore maintenance actions are expensive and should be minimized or even avoided in order to keep the LCOE low. Therefore, it is desired to use maintenance-free bearings for WEC applications.

Depending on the application and the bearing type, there are different causes for contact bearing failures. Figure 1 shows examples of the causes for bearing failures. This flow chart is partly based on the information given in [15]. In general, there are two failure modes: mechanical failure and tribological failure. Both failure categories are time dependent, but the mechanical failure is mainly driven by the load cycles and the tribological failure by the motion of the two surfaces in contact over time.

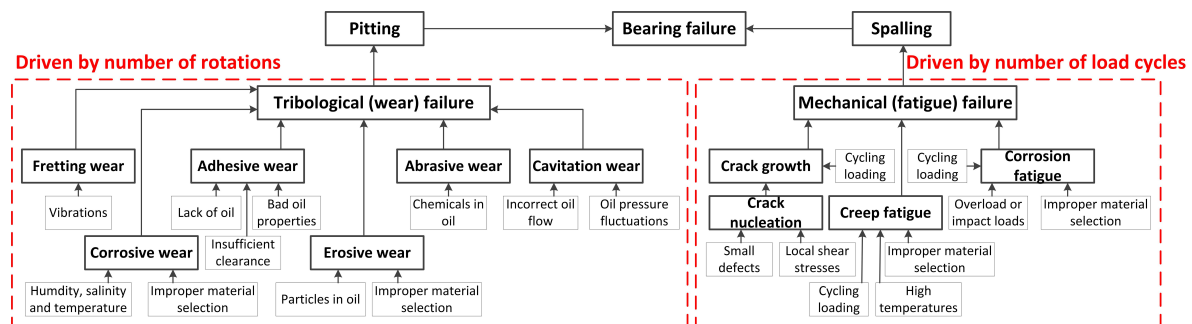


Figure 1. Example causes for bearing failures partly based on [15].

Deterioration mechanisms for wear and fatigue are complex and caused by different processes. Tribological failures (wear failures) may dominate when having high-speed bearings/shafts with many full rotations of the shaft. Fatigue failure modes can be assumed to be dominating when a low number of rotations is carried out (low wear), but a high number of load cycles, leading to unequally loaded sections of the bearing. For mechanical engineering applications where high-speed shafts are commonly used, like in power plants (see, e.g., [16,17]) or airplane engines (see, e.g., [18]), the focus when designing bearings is mainly on wearing problems (e.g., by measuring the resulting axial and radial play of a bearing). For civil engineering applications, like bridges (see, e.g., [19]), bearing failure is often described by a fatigue modeling approach. Often, a combination of fatigue failures, as well as tribological failures occurs due to the complexity of the overall failure (wear and crack evolution) progress. Stress concentrations, which increase during the expected lifetime inside the bearing, may

lead to local overload of the bearing and then to structural collapse at an early stage due to accelerated crack evolution driven by large local load amplitudes.

Another way to characterize primary causes of bearing failures can be based on observable different conditions, as shown in [20,21]:

- Excessive load,
- Overheating,
- (False and true) brinelling,
- Normal fatigue failure,
- Reverse loading,
- Contamination,
- Lubricant failure,
- Corrosion,
- Burns from electric current,
- Misalignment,
- (Loose and tight) fits.

Failure analysis of bearings is complicated due to the fact that one failure mode may initiate another. The different bearing failure modes will have different time-dependent limit state functions. In a first step towards minimizing bearing failure, the process should include avoiding the wrong installation (e.g., misalignment), contamination, inadequate lubrication (the wrong type of lubricant or an insufficient amount of lubricant), as well as misuse of the bearing.

Which failure modes ought to be considered in a certain case generally depend on the application for which a certain bearing is used, as well as the environmental conditions in which it is operating. For WEC applications, the load cycle frequencies are in the range of the passing waves. Often, not full rotations are executed at the bearing, but the two interconnected structural elements are swinging in relation to each other. The load changes when a wave is passing are large, but the resulting rotation of the bearing elements can often be assumed to be low. This means that a limiting factor for many bearings installed in WECs is not the rotations due to passing waves, but the load changes due to passing waves leading to mechanical fatigue failure. Due to the fact that the diversity of the working principles for harvesting energy from waves is large, the above statement may not be valid for all working principles.

4. The Wavestar Device

The Wavestar device is a WEC, which contains floaters moving due to passing waves and driving a hydraulic cycle. The fluctuating oil flow impels a turbine and a generator that produces electricity. The rated power of one floater is equal to 55 KW, and a prototype was installed at Hanstholm on the west coast of the Danish North Sea. Figure 2 shows a picture of the prototype and the location on the device investigated. This paper analyzes the bearing connection of the floater arm and the PTO rod. In order to decrease the loads on the structure in the case of extreme environmental conditions, the floaters can be moved out of the water. This prototype was in service and feeding electricity into the Danish electricity grid between January 2010 and September 2013. At the moment, remodeling work is ongoing, and two additional floaters with a diameter equal to 6 m were installed on the existing prototype.

Furthermore, it is planned to install a new PTO system to get higher efficiencies of the conversion process due to decoupling of the electricity production from the pressure fluctuations in the hydraulic cycle when waves are passing. More information about the new PTO system, which is being tested in a real-scaled test-bench, is available in [10]. The main novelty of this new PTO system consisting of a discrete displacement cylinder (DDC) is to smoothen the pressure fluctuations within the pressure cycles by having three separated pressure cycles. This system enables having a smoother electricity production over time. The multi-chambered cylinders contain main valves, which have many opening and closing actions. Each closing/opening of the valves leads to pressure fluctuations

within the hydraulic cycle, leading to small load fluctuations of a step function shape on the structure of the floater and the PTO rod. The load calculations in the considered case study are based on a Simulink model, which models the new DDC PTO system. Information about the Simulink model can be found in [22,23]. Figure 3 shows an example (bearing load and movement of the floater) of a part of a time series. This study considers a single floater device.



Figure 2. Wavestar prototype located at Hanstholm (Denmark) showing the location of the investigated bearing. Power take-off: PTO.

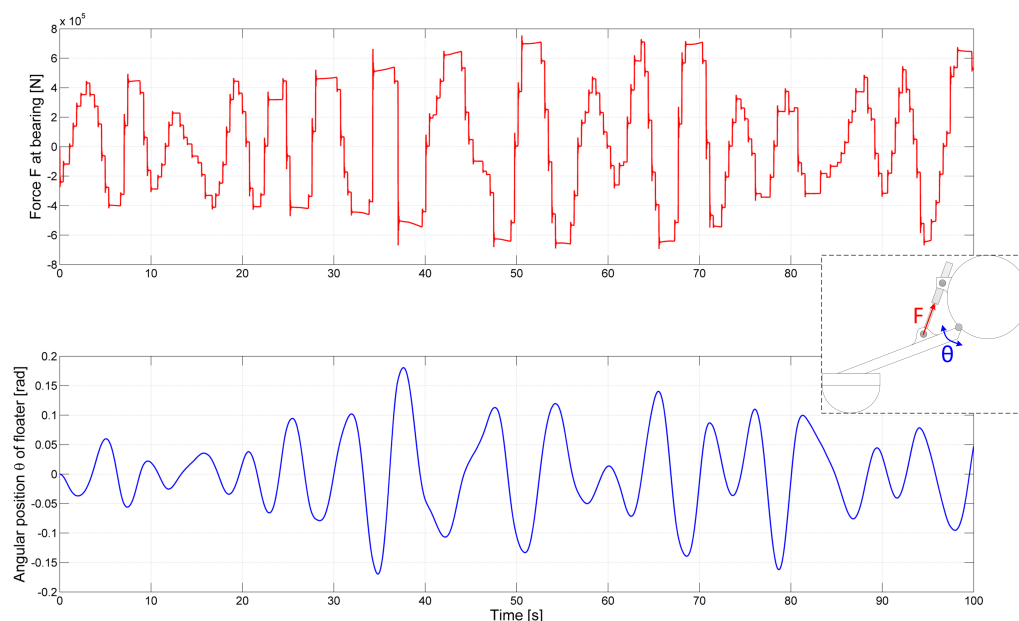


Figure 3. Detail of a time series example (here, $H_{m0} = 3.25$ m; $T_{0,2} = 5.5$ s) of the simulations showing the bearing load F , as well as the angular position θ of the floater. H_{m0} : significant wave height; $T_{0,2}$: mean wave period.

Table 2 and Figure 4 respectively show the considered scatter diagram of the considered wave conditions, as well as the incoming wave direction distribution. The device is producing electricity when the significant wave height is between 0.5 m and 3.5 m. For significant wave heights smaller

than 0.5 m, the floaters are taken out of the water due to the fact that the low electricity production is non-economical. The incoming wave distribution is split into 16 sections (see Figure 4), each covering a range of 22.5°.

Table 2. Scatter diagram with the probabilities of occurrence (given here in percent) of the different wave states. Numbers in red mean that the device is in idle mode (no electricity production).

	Mean Wave Period $T_{0,2}$ (s)		
	3.0–4.0	4.0–5.0	5.0–6.0
< 0.5	10.7	3.1	-
0.5–1.0	19.4	12.2	-
1.0–1.5	6.9	17.2	-
1.5–2.0	-	11.1	5.9
2.0–2.5	-	3.2	4.1
2.5–3.0	-	-	3.4
3.0–3.5	-	-	2.7

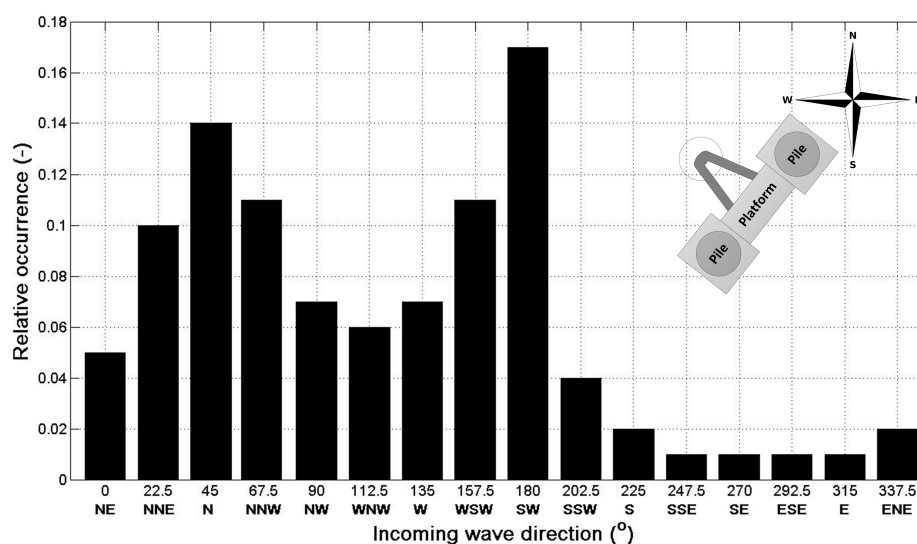


Figure 4. Probabilities of occurrences of different incoming wave directions.

Plain bearings are planned to be installed at the considered location due to the fact that this bearing (Figure 2 shows its location) has no full rotations, but many load cycles due to passing waves. This article considers fatigue failure (mechanical failure) of the plain bearing. This investigation does not assume any misuse, contamination or wrong installation. Furthermore, the considered plain bearings do not need maintenance actions, and it is assumed that the material properties remain the same over time, as well as the number of cycles are the same for all of the years. Failure of the considered bearing location may lead over time to partial collapse of the floater structure, to the inability of moving the floater out of the water (into idling mode), as well as the inability of producing electricity.

The reliability of different plain bearings shown in Table 3 is investigated for the Wavestar prototype using the new PTO system. The considered plain bearings, which are available from stock, have a dry lubricant polytetrafluoroethylene (PTFE), and the rest (inner and outer ring) is made out of GCr15 steel with Grade E40. The dry lubricant is one of the materials with an extremely low friction coefficient, and dry lubrication is used in order to decrease the maintenance costs.

Table 3. Considered plain bearing types (GE-type bearings from Schaeffler). The dimension values are taken according to [24], and the prices are taken from [25]. The exact meaning of the diameter values D_i and D_a can be seen in Figure 5.

Meaning	Type of Bearing				
	GE60 UK	GE70 UK	GE80 UK	GE90 UK	GE100 UK
Inner bearing diameter D_i (mm)	60	70	80	90	100
Bearing diameter D_a (mm)	70.9	82.4	94.2	103.1	116.3
Width l (mm)	36	40	45	50	55
Price (\$)	286	407	531	685	1023
Normalized price (-)	1.00	1.43	1.86	2.40	3.58

This reliability assessment focuses on a specific detail at the Wavestar device. However, a structural reliability analysis at the considered location (see Figure 2) is of importance due to the fact that this bearing is difficult to replace (needs many man hours and special equipment with a crane). Therefore, the bearing should be designed in order to hold for the overall expected lifetime of 20 years, and no replacements of the bearing during the expected lifetime of the device are planned. Offshore operation and maintenance actions can be expensive due to limited accessibility (weather conditions) and the long transportation times. The work in [26] gives an overview of different operation and maintenance strategies applicable to WEC technologies.

The price differences for a single bearing (see Table 3) might be negligible when comparing it to the overall investment cost of the device. However, one floater needs four bearings (one for the PTO cylinder (floater), one for the PTO cylinder (platform and two for floater) platform connection), and the planned device consists of 20 floaters [5]. In this case, the bearing expenses and their potential savings are no longer negligible. In addition, there is a series system effect, because failure of one bearing implies that a repair is needed, and the device is stopped (no electricity production).

5. Considered Fatigue Model

Dynamic simulations are of importance for fatigue load assessments due to the fact that no full rotations of the bearing are performed in the considered study, and therefore, unequally-distributed loads along the bearing ring occur. Furthermore, many stops and load direction changes are performed as the floater and the PTO cylinder are moving upwards and downwards when a wave is passing.

No detailed information about the specific EGOGLIDE® lubrication layer is available. Therefore, no detailed and representative local load estimation has been performed at the bearing. The surface friction loads resulting from the dynamic simulations are assumed to be sinusoidally-distributed. This simple load assessment is of course related to the uncertainties, which will be introduced in a later step (see Section 5.2) when probabilistic reliability assessments are performed.

For fatigue modeling, the circumferential pressure distributions are needed in order to model the elongation of cracks, which occur on and below the surface. The bearing pressure p applied on the bearing is assumed to be uniformly distributed along the width l of the bearing (see Figure 5):

$$p = \frac{L}{D_a \cdot l} \quad (4)$$

where D_a is the diameter of the bearing (the diameter where friction between the inner and outer ring takes place (see Figure 5)) and L the applied load resulting from the motion of the floater. In order to estimate the friction loads at the surface of the inner bearing ring, the perpendicular loads on the surface need to be estimated. Maximum shear is assumed to occur at the contact surface between the inner and outer ring of the bearing. This assumption is in accordance with [27] when the friction

coefficient is equal to or larger than 0.1. Therefore, it is assumed that the cracks are developed from the surface. The perpendicular compression pressure p_c can be calculated as:

$$p_c = p \cdot \cos(\alpha) \quad (5)$$

where α is the position angle shown in Figure 5, which gives an overview about the considered parameters and pressure distributions. The local shear stress τ can be calculated from the local compression pressure, p_c , as follows (Coulomb friction law):

$$\tau = p_c \cdot \mu \quad (6)$$

where μ is the friction coefficient.

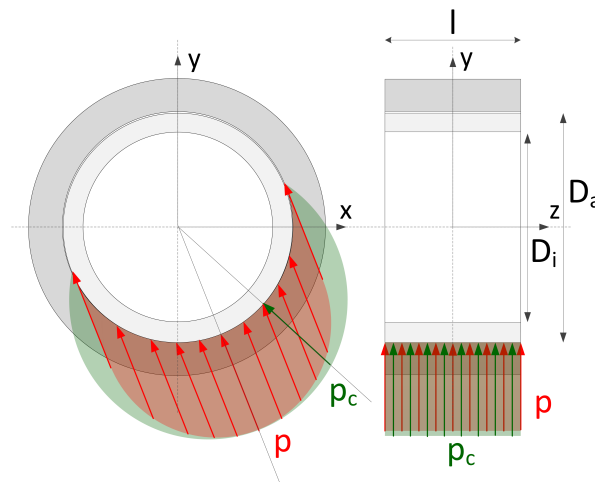


Figure 5. Coordinate system and the considered parameters: p : pressure distribution; p_c : compression pressure; l : length/width bearing; D_i : inner diameter bearing; D_a : bearing diameter; α : position angle.

Figure 6 shows a flow chart of the procedure to assess the fatigue shear and compression pressure distributions used for fatigue modeling. The loads at the bearing are dependent on the environmental conditions, which are represented by a scatter diagram (Table 2) and the incoming wave direction distribution, as shown in Figure 4. Based on the environmental conditions, load time series are generated for the different wave conditions. These load time series are converted into shear and compression pressure time series of a certain bearing segment. Due to unequal load distributions and not full rotations of the bearing, there will be large local pressure differences among bearing ring. This needs to be accounted for based on a dynamic simulation and is done by dividing the bearing ring into segments where the local pressure time series are identified for each wave conditions and for each bearing segment. Figure 7 shows how the inner bearing ring is diverted into segments. In the current study, the bearing ring is diverted into 90 segments (each segment covers four degrees).

For fatigue assessments, it is the cycle amplitudes, not the instantaneous stresses, that are important. Therefore, for each load time series, rainflow counting (see, e.g., [28]) is performed in order to estimate the local stress amplitude spectrum from a certain pressure time series. The stress ratio (R ratio) is not considered in this damage model, as this ratio will be different for each considered segment. However, the R-ratio can be included in the rainflow counting process. The overall (mean) stress spectrum is based on the wave conditions (environmental conditions), as well as weighted with the number of segments. The following section will explain in greater detail how the stress distributions are estimated

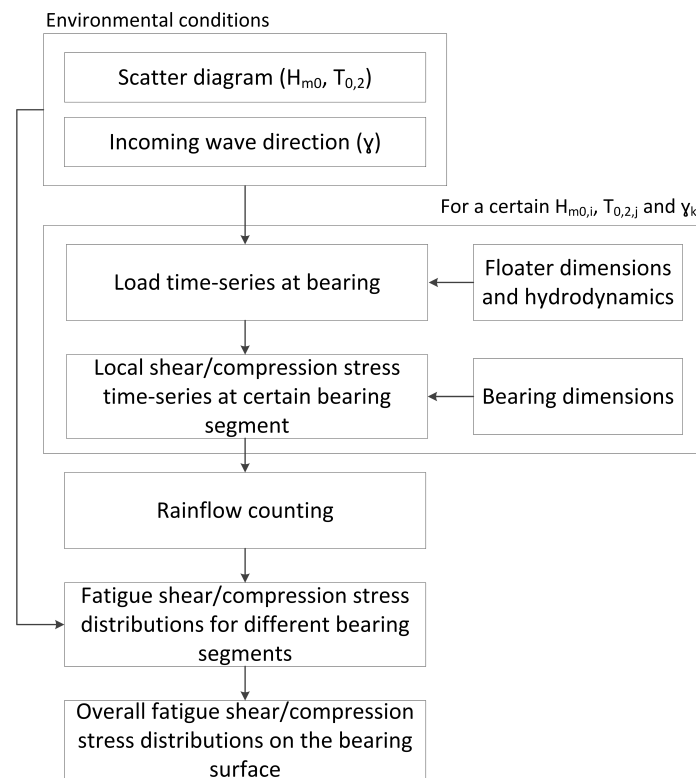


Figure 6. Flow chart of the procedure to calculate fatigue surface stresses at different locations on the bearing surface.

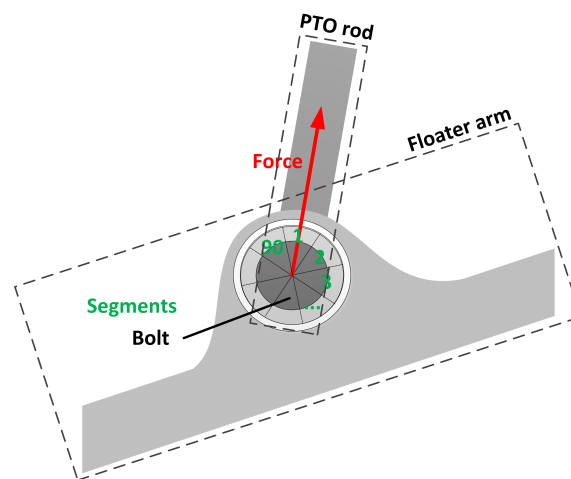


Figure 7. Sketch of the considered plain bearing segments.

5.1. Considered Limit State

Intergranular brittle fracture originating at the bearing surface is according to [29] an important failure mode for GCr15 steel bearings due to their relatively high amount of carbon. This article considers this failure mode as the bearing material of the considered bearing types consisting of high-carbon chromium bearing steel GCr15 and PTFE-based material as the lubricant. The threshold value for crack growth, which gives the threshold at which a small crack begins to grow, can explain the ability of a material to resist growing cracks. This crack growth threshold, K_{th} , is an important parameter for brittle fatigue considerations.

When considering very high cycle fatigue (also called gigacycle fatigue) and using GCr15 bearing steel where the life regime is beyond 10^7 cycles, the majority of the fatigue life (more than 90%) is according to [30] corresponding to crack initiations and the coalescence of very small cracks to cracks that can grow. Therefore, in order to define a limit state, the threshold (K_{th}) for crack growth can be used as the limit state for this kind of material, because, as mentioned earlier, the largest part of the expected lifetime is most used to initiate cracks. This approach is only applicable if the crack growth rate is large, as well as the time is small between crack initialization and structural failure compared to the expected lifetime. For other materials where the time between crack initialization and structural failure is not negligible, the threshold SCF as limit state would be too conservative. In such cases, also the time when the crack is growing needs to be considered. The exceedance of the threshold for crack growth per stress cycle is considered here as the failure mode. This means if the crack starts to grow, it will always lead to structural failure. The corresponding limit state equation can be written as [31]:

$$g(X) = K_{th} - X_{WS} \cdot X_{WL} \cdot K_{eq} \quad (7)$$

where K_{th} is the theoretical/experimental threshold for critical crack growth, X_{WS} the uncertainty about the wave conditions and X_{WL} the uncertainty related to the load calculation given a certain wave state. The equivalent stress intensity factor, K_{eq} , can be calculated as:

$$K_{eq} = f(a, p_c, \alpha) = (Y_n \mu p_c X_{mn} + Y_c p_c X_{mc}) \cdot \sqrt{\pi a} \cos(\alpha) \cdot X_{SCF} \quad (8)$$

where a is the crack depth, which is equal in this case to half the crack width, p_c is the tangential pressure cycle amplitude, Y_c , as well as Y_n are the SCFs for compression loads, as well as sliding (surface friction). The uncertainties related to the SCFs Y_c and Y_n are named X_{mc} and X_{mn} , respectively. The parameter α indicates the crack direction relative to the force. Figure 8 shows the orientation of the angle α on the bearing ring. The stochastic parameter X_{SCF} represents the stress concentration uncertainty given a certain load.

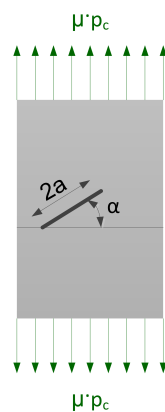


Figure 8. Direction of the orientation of angle α on the surface of the bearing ring.

Due to the fact that the bearing ring is diverted into N segments, the equivalent stress intensity factor K_{eq} representing all N segments can be estimated by an expansion of Equation (8), taking into account the local stress distributions of the different segments:

$$K_{eq} = \frac{1}{N} f(a, p_c, \alpha) = \frac{(Y_n \mu X_{mn} + Y_c X_{mc}) \cdot \sqrt{\pi a} \cos(\alpha) \cdot X_{SCF}}{N} \sum_{i=1}^N p_{c,i} \quad (9)$$

where $p_{c,i}$ is the stress cycle distribution at section i and N the number of sections into which the bearing is divided. The equivalent stress intensity factor K_{eq} in Equation (9) is considered for

the probabilistic reliability assessment and represents the average over all local stress ranges of the N segments in order to make the considered equivalent stress intensity factor independent of the number of considered segments. The stress cycle distribution can be determined from stress time series by the aid of rainflow counting. Rainflow counting gives the number of stress cycles given a certain stress amplitude. How the load time series are analyzed to get the number of load cycles is, e.g., given by [28]. Figure 9 shows, as an example, two different surface pressure spectra for two different segments at the inner bearing ring. These two segments have different surface pressure distributions, which make different pressure spectra at different locations on the bearing ring necessary in order to define the equivalent stress intensity factor, K_{eq} , as shown in Equation (9).

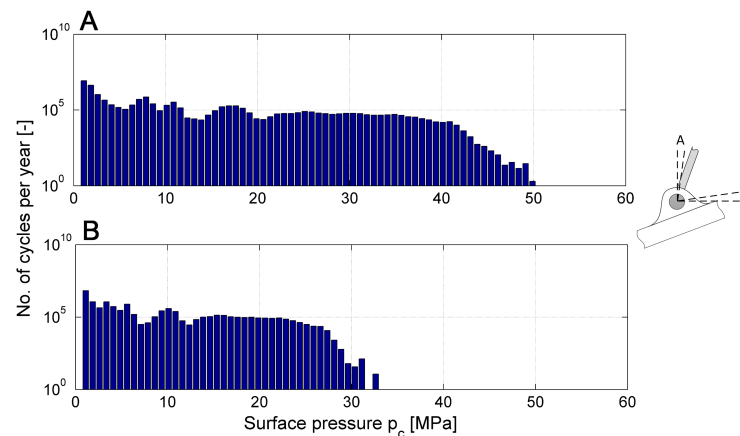


Figure 9. Example of a fatigue surface pressure range spectrum at two different locations at the bearing ring (Segments A and B). The diameter of the inner bearing ring is in this example 100 mm.

The SCFs Y_c and Y_n from Equation (8) can be calculated according to [32]:

$$Y_c = g \left[0.923 + 0.199 \left[1 - \sin \left(\frac{\pi a}{2D_a} \right) \right]^4 \right] \quad (10)$$

$$Y_n = g \left[0.752 + 2.02 \left(\frac{a}{D_a} \right) + 0.37 \left[1 - \sin \left(\frac{\pi a}{2D_a} \right) \right]^3 \right]$$

where D_a is the bearing diameter (see Figure 5), a the crack depth and g a constant, which is equal to:

$$g = \frac{1.84}{\pi} \left[\tan \left(\frac{\pi a}{2D_a} \right) / \left(\frac{\pi a}{2D_a} \right) \right]^{0.5} \quad (11)$$

$$\cos \left(\frac{\pi a}{2D_a} \right)$$

From the limit state equation (see Equation (7)), the probability of failure, P_F , per load cycle is estimated by using FORM techniques. In order to compare the failure probability with the maximum acceptable failure rates of WEC components, the annual failure probability, ΔP_F needs to be found by:

$$\Delta P_F = N_{annual} \cdot P_F \quad (12)$$

where N_{annual} is the number of load cycles per year. Commonly, the annual reliability index $\Delta\beta$, which can be derived from the annual probability of failure (see Equation (2)), is considered for comparing the structural reliability of different structural designs. The probability of failure calculated in this example can be understood as the upper bound of the structural failure probability, as only the time until the crack starts growing is considered, and the short time, while the crack is growing,

is disregarded here (see Equation (7)). Since failure occurs at an extremely large stress range, it is alternatively possible to use a stochastic model based on the annual maximum load range.

5.2. Stochastic Model

Table 4 shows the considered values of the parameters of the stochastic model for the brittle fracture fatigue failure of a plain bearing as presented in Equation (7). For K_{th} , the coefficient of variation (COV) value and distribution type are taken from [14], whereas the mean value of $4.5 \text{ MPam}^{0.5}$ is taken from [33]. The crack depth is assumed to be log normal distributed [14]. The model uncertainties, X_{mn} and X_{mc} , related to the equivalent stress intensity factors (physical model) Y_n and Y_c , are chosen according to [14] with a COV equal to 0.2. The COV value of uncertainty about wave conditions, X_{WS} , can be set equal to 0.15 if different incoming wave directions are considered and more than one year of wave data is available (see, e.g., [6,34]). The uncertainty about the stress concentration given a certain load onto the structure, X_{SCF} , has a COV value equal to 0.15 (see [6,35]) when a parametric equation is used to calculate the SCFs Y_n and Y_c . The wave load calculation uncertainty, X_{WL} , is assumed to have a COV value between 0.1 and 0.2. The mean period of a wave (at the considered location) is equal to 5.75 s. This leads to an annual number of cycles equal to 5.485×10^6 . The crack orientation angle α is assumed to be uniformly distributed within the interval $[-\frac{\pi}{2}; \frac{\pi}{2}]$. The friction coefficient μ is according to [36] assumed to be log normal distributed. The expected friction coefficient between steel and PTFE is between 0.05 and 0.2 (see, e.g., [37]). The COV value of μ is set equal to 0.15, which is in accordance with the former friction studies (see, e.g., [36]).

Table 4. Stochastic model for the reliability analysis of plain bearings for the Wavestar device. LN: log normal; COV: coefficient of variation; SCF: stress concentration factor.

Name	Description	Type	Stochastic Model		Source
			Expected Value	COV	
K_{th}	Threshold for crack growth	LN	$4.5 \text{ MPam}^{0.5}$	0.4	[14,33]
a	Crack depth	LN	0.15 mm	0.66	[14]
α	Crack orientation	uniform	0	$\frac{\pi}{\sqrt{12}}$	
μ	Friction coefficient (dry lubricant)	LN	(0.05...0.1...0.15...0.2)	0.15	[36,37]
X_{mn}	Model uncertainty Y_n	LN	1	0.2	[14]
X_{mc}	Model uncertainty Y_c	LN	1	0.2	[14]
X_{SCF}	Stress concentration factor uncertainty	LN	1	0.15	[6,35]
X_{WS}	Uncertainty wave conditions	LN	1	0.15	[6,34]
X_{WL}	Uncertainty wave load calculations	LN	1	(0.1...0.15...0.2)	[14]

The surface stress cycle distribution $p_{c,i}$ as shown in Figure 9 is assumed to be Weibull distributed, which is widely used in fatigue modeling (see, e.g., [38]). The considered Weibull distribution consists of two parameters called scale parameter a and shape parameter b . The distribution function of a two-parameter Weibull distribution looks like:

$$F_i(p_{c,i}|a, b) = 1 - \exp\left(-\left[\frac{p_{c,i}}{a}\right]^b\right) \tag{13}$$

The Weibull parameters are fitted using a maximum likelihood approach, and for each Weibull fit, a time series length of 1000 waves is considered. However, before starting to fit the distributions, it is necessary to prove their quality and accuracy of fit. This can be done with a Q-Q plot (quantity-quantity plot), where the theoretical values from the distribution are plotted on the x-axis and their corresponding exact sample values on the y-axis. The better the distribution represents reality, the closer are the resulting coordinates along the bisecting line. Figure 10 shows an example of a Q-Q plot of a Weibull distribution of a segment. The considered surface stress load spectrum

shows the appropriate fit with a Weibull fit. This means that the Weibull distribution is able to represent the behavior of the load cycle characteristics in an appropriate manner and to justify the use of a Weibull distribution for fatigue modeling. The deviations between the fitted and the real data shown in Figure 10 are considered in the stochastic variable X_{WL} , which covers uncertainties related to simplifications in wave load calculations and fitting uncertainties.

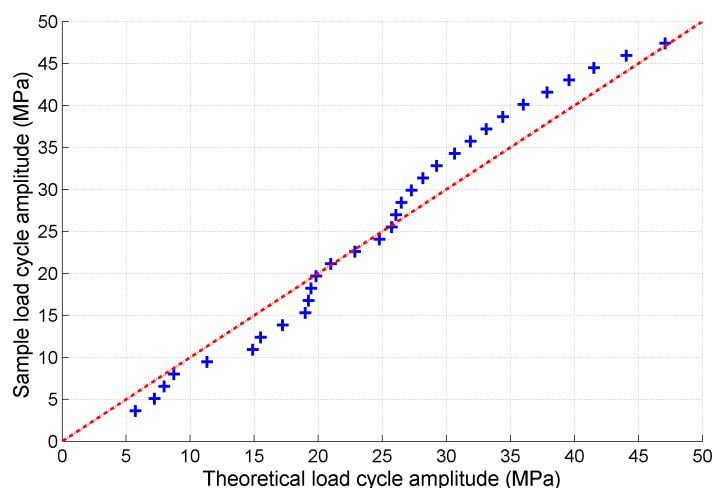


Figure 10. Example of the Q-Q (quantity-quantity) plot of a surface stress cycle Weibull distribution fit to the load cycle for one segment ($D = 80$ mm).

The overall reliability calculation process includes three steps. The first step involves transferring the general load time series to surface stress time series for the different segments, taking into account the motion of the floater. The next step involves performing rainflow counting and fitting a Weibull distribution to the resulting stress spectra. Step 3 includes the probabilistic reliability analysis by using the MATLAB-based FERUM (finite element reliability using Matlab) simulation tool [39] in order to estimate the probability of structural bearing failure considering brittle fatigue failure.

6. Results

A parametric study presents the results in which different sensitivity analyses of uncertain parameters are performed. Considered in this parametric study are the following parameters:

- Wave load X_{WL} uncertainty range,
- Mean crack size a ,
- Friction coefficient μ ,
- Number of annual load cycles (N_{annual}).

The following sections will include discussions on the influence of the above-mentioned parameters on the annual reliability index.

6.1. Influence of Wave Modeling Uncertainty X_{WL}

Due to the fact that the uncertainty related to wave load uncertainties is unknown in this specific example, the wave modeling uncertainty needs to be estimated and is assumed to have a COV between 0.1 and 0.2, which is in accordance with the proposed load modeling uncertainties in [14]. The uncertainty X_{WL} considers simplifications related to the wave load modeling, as well as fitting uncertainties of the surface stress cycle distribution $F_i(p_{c,i})$.

Figure 11 shows the resulting annual reliability index for plain bearings with different inner bearing radii D_i (between 60 mm and 100 mm) dependent on the wave modeling load uncertainty

X_{WL} . A smaller radius generally leads to smaller annual reliability indices for a given wave modeling uncertainty due to the fact that a smaller radius leads to larger local stresses. Furthermore, the influence of the radius is more important than differences in the COV value of the wave load uncertainty.

As discussed earlier, the minimal required annual reliability index of the components used for WEC applications should have a value between 3.1 and 3.7. If one requires a minimal reliability index of at least 3.1, the bearing GE80 UK with a bearing diameter of 80 mm should be used. In case a minimal annual reliability index equal to 3.7 is required, the bearing UK90 UK with a bearing diameter of 90 mm should be taken. For this application, the plain bearings GE60 UK and GE70 UK lead to unacceptable high annual failure probabilities (low annual reliability indices) and should not be mounted on the Wavestar device to connect the PTO system with the floating arm.

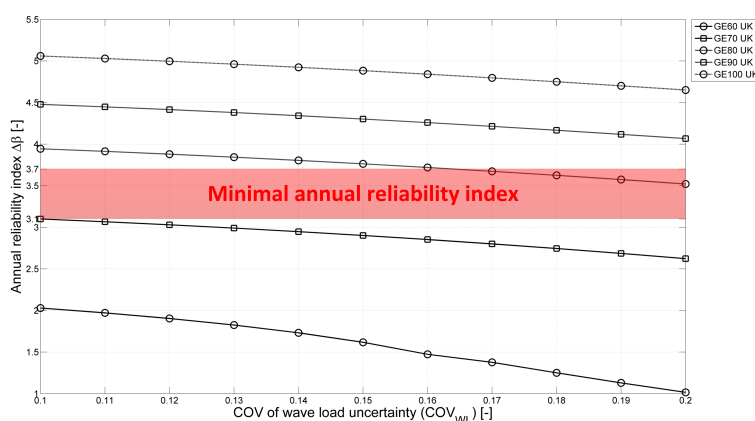


Figure 11. Annual reliability index for the mechanical failure of different bearings dependent on the COV value of the wave load uncertainty X_{WL} . The mean value of friction coefficient μ is set equal to 0.15.

6.2. Influence of Mean Crack Size a

The mean crack size, which is used to calculate the equivalent stress intensity factor, K_{eq} (see Equation (8)) depends on steel material characteristics defined by the steel quality, as well as the chemical composition of the used steel. The mean crack size of 0.15 mm given in [14] is a value that can be used for all different steel types. No explicit data for the GCr15 steel is available, and therefore, this section will include a sensitivity analysis varying the mean crack size from 0.1 mm to 0.2 mm.

Figure 12 shows the annual reliability index for the bearing GE80 UK and GE90 UK dependent on the mean crack size. As expected for both bearing types, larger mean crack sizes lead to lower resulting annual reliability indices. For this investigation, the COV value considering wave load modeling, X_{WL} , is fixed at 0.15.

The minimal annual reliability index of the GE90 UK bearing remains for the considered mean crack size range always above 3.7, whereas the annual reliability index of the GE80 UK bearing moves below 3.7 for larger mean crack sizes than 0.15 mm, but always remains above 3.1. If the minimal acceptable reliability level is set equal to 3.1, the smaller bearing GE80 UK is sufficient for the considered failure mode, whereas when a minimal annual reliability index equal to 3.7 is demanded, the larger bearing GE90 UK should be mounted.

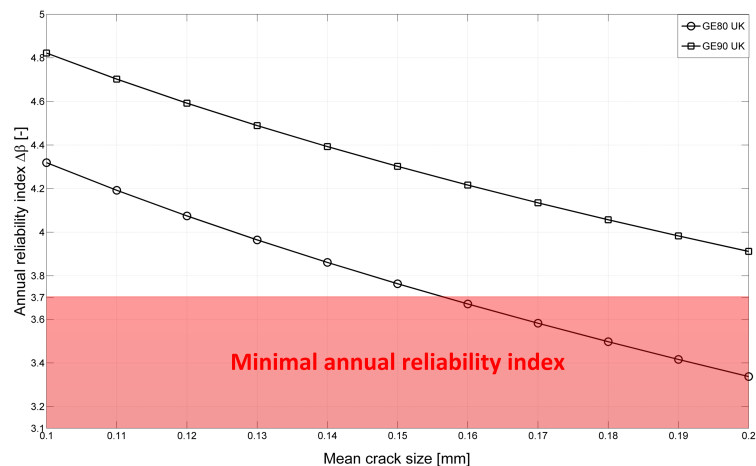


Figure 12. Annual reliability index for different bearings dependent on the mean crack size a . The mean value of friction coefficient μ is set equal to 0.15, and the COV value of the crack size is set constant at 0.66.

6.3. Influence of Friction Coefficient μ

The expected friction coefficient between PTFE and steel is according to [37] in the range between 0.05 and 0.2. The expected friction coefficient between steel and PTFE surfaces has a large range, and no specific information about the considered bearings is available. Therefore, this section will investigate the influence of the mean friction coefficient on the annual reliability index.

The sensitivity of the annual reliability dependent on the friction coefficient is shown in Figure 13 for the two bearing types GE80 UK and GE90 UK. The mean friction coefficient is varied between 0.05 and 0.2, whereas the COV of the friction coefficient remains constant at 0.15.

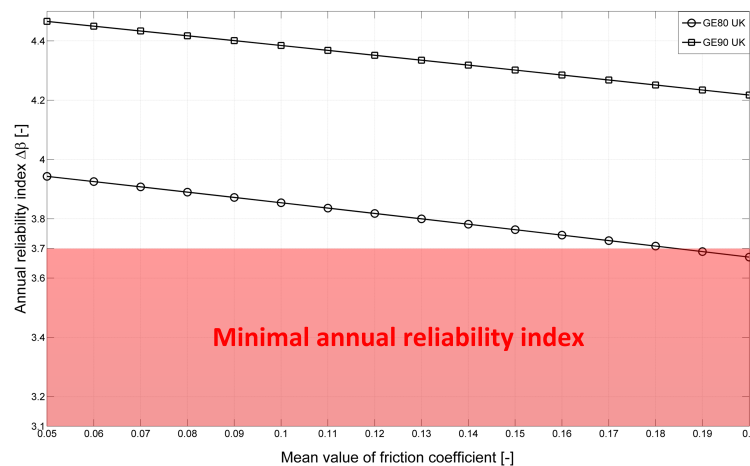


Figure 13. Annual reliability index for different bearings dependent on the mean friction coefficient μ . The mean value crack size a is set equal to 0.15 mm; the COV of the expected friction coefficient remains constant at 0.15 and the COV value of X_{WL} equal to 0.15.

The annual reliability index decreases linearly from 4.45 to 4.20 and from 3.95 down to 3.65 for the bearings GE90 UK and GE80 UK, respectively, when the mean friction coefficient is increased from 0.05 to 0.2. In the case where the friction coefficient is lower than or equal to 0.18, the GE80 UK bearing would be sufficient for a requested minimal reliability index of 3.7. Whereas for large friction values, the larger bearing GE90 UK should be taken.

6.4. Influence of Annual Number of Load Cycles N_{annual}

The study performed so far is dependent on the location, which is characterized by the scatter diagram (including the probability of occurrences of the different wave states). Different scatter diagrams will lead to different annual numbers of load cycles, N_{annual} , to be expected. This section investigates the impact of different N_{annual} values on the structural reliability.

Figure 14 shows the annual reliability index dependent on the annual number of cycles for the two bearings GE80 UK and GE90 UK, respectively. The sensitivity to the considered annual number of load cycles is estimated based on varying the calculated annual number of cycles for the Wavestar at Hanstholm by $\pm 20\%$. Compared to the other considered parameters, like the wave load uncertainty X_{WL} , the expected value of the friction coefficient μ and the mean crack size a , the impact on the annual reliability index for different N_{annual} values is small.

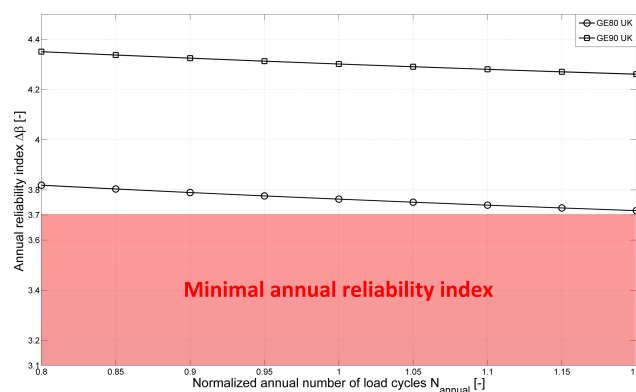


Figure 14. Annual reliability index when changing the annual number of cycles between 80% and 120% of the originally determined N_{annual} . The mean value crack size a is set equal to 0.15 mm, the expected friction coefficient equal to 0.15 and the COV value of X_{WL} equal to 0.15.

7. Conclusions

This paper focuses on structural reliability assessments of plain bearings for WEC applications. A probabilistic reliability approach is used to estimate the probability of failure of different plain bearings. Probabilistic reliability assessments account for uncertainties related to Mother Nature (physical uncertainties), model uncertainties, limited dataset lengths (statistical uncertainties) and measurement uncertainties. Here, this article presents a methodology for brittle fatigue failure of surface-induced stresses based on friction and compression loads from the waves and applies it to a case study.

The chosen case study is the Wavestar device, which is placed at the Danish west coast of the North Sea. Future Wavestar devices will use plain bearings between the floater and the PTO cylinder. They should also include the implementation of a new developed PTO system, which is based on so-called DDCs, which smoothen the pressure fluctuations within the hydraulic cycle in order to increase the conversion efficiency of the harvested energy into electricity. The new PTO system also leads to different load characteristics compared to the current Wavestar PTO design and, therefore, to different structural designs.

Sensitivity analyses for unknown parameters, like the wave load uncertainty range, the crack size, the friction coefficient within the bearing and the number of annual load cycles, are performed in order to understand the validity of the outcome, the adaptability to other locations, as well as the use of other bearing materials. The results indicate that uncertainties related to wave load assessments and the considered failure mode model have a larger impact on the structural reliability than uncertainties related to different wave resources at different locations.

For WEC components, the annual target reliability levels should be between 3.7 and 3.1, which correspond to an annual failure probability between 10^{-3} and 10^{-4} . The target reliability levels are defined based on the consequences in the case of structural failure, which are only of monetary value for WEC devices, and there is no danger of human fatalities, as well as no large environmental pollution.

The considered case study investigates different plain bearings from stock. For a target reliability index equal to 3.1, the plain bearing (called GE80 UK), with an inner bearing diameter equal to 80 mm, achieves the required conditions when focusing on friction and compression load-induced fatigue. For a larger target reliability index equal to 3.7, a larger plain bearing (called GE90 UK), with an inner bearing diameter equal to 90 mm, should be used for the Wavestar device.

This paper only considers one possible bearing failure mode. Fatigue failure is of importance for WEC components exposed to cyclic loading due to passing waves. There are also other failure modes, which might be important for this application, such as, e.g., abnormal loads due to the wrong installation or wrong selection of the bearing type, as well as quality/production mistakes or misalignment due to large radial loads.

Acknowledgments: The authors wish to thank the financial support from the ForskEL - energinet.dk research program (Contract 12155, 'Digital Hydraulic Power Take Off for Wave Energy') which made this work possible.

Author Contributions: Simon Ambühl developed together with John D. Sørensen the methodology for estimating the reliability of the plain bearing. Simon Ambühl and John D. Sørensen did the reliability calculations. Morten Kramer developed the Simulink model of the Wavestar device delivering load time series at the PTO rod of the Wavestar device. Simon Ambühl performed the detailed simulations with a focus on the bearing based on the general load time series from the Simulink model. Simon Ambühl wrote the paper draft. Morten Kramer and John D. Sørensen revised the paper draft, and Simon Ambühl updated the paper according to their review.

Conflicts of Interest: The authors declare no conflict of interest.

References

1. De O. Falcão, A.F. Wave energy utilization: A review of the technologies. *Renew. Sustain. Energy Rev.* **2010**, *14*, 899–918.
2. Güneş, M.S.; Kaygusuz, K. Hydrokinetic energy conversion systems: A technology status review. *Renew. Sustain. Energy Rev.* **2010**, *14*, 2996–3004.
3. Christensen, L.; Friis-Madsen, E.; Kofoed, J.P. The Wave Energy Challenge: The Wave Dragon Case. In Proceedings of the POWER-GEN 2005 Europe Conference, Milan, Italy, 20–21 October 2005.
4. Thorpe, T.W. *A Brief Review of Wave Energy*; Harwell Laboratory, Energy Technology Support Unit: London, UK, 1999.
5. Kramer, M.; Marquis, L.; Frigaard, P. Performance evaluation of the Wavestar prototype. In Proceedings of the 9th European Wave and Tidal Conference (EWTEC), Southampton, UK, 5–9 September 2011.
6. Ambühl, S.; Ferri, F.; Kofoed, J.P.; Sørensen, J.D. Fatigue reliability and calibration of fatigue design factors of wave energy converters. *Int. J. Mar. Energy* **2015**, *10*, 17–38.
7. Ambühl, S.; Kramer, M.; Kofoed, J.P.; Sørensen, J.D. Reliability assessment of wave energy devices. In Proceedings of the 4th International Conference on Ocean Energy (ICOE), Dublin, Ireland, 17–19 October 2009.
8. Márquez-Domínguez, S.; Sørensen, J.D. Fatigue reliability and calibration of fatigue design factors for offshore wind turbines. *Energies* **2012**, *5*, 1816–1834.
9. *Tidal Turbines*; DNVGL-ST-0164; DNV GL A/S: Høvik, Norway 2015.
10. Hansen, R.H.; Kramer, M.M.; Vidal, E.V. Discrete displacement hydraulic power take-off system for the Wavestar wave energy converter. *Energies* **2013**, *6*, 4001–4044.
11. Hansen, R.; Kramer, M. Modelling and control of the Wavestar Prototype. In Proceedings of the 9th European Wave and Tidal Conference (EWTEC), Southampton, UK, 5–9 September 2011.
12. Madsen, H.O.; Krenk, S.; Lind, N.C. *Methods of Structural Safety*; Dover Publication, Inc.: Mineola, NY, USA, 1986.

13. Lemaire, M. *Structural Reliability*; International Society for Technology in Education (ISTE) Ltd.: London, UK, 2009.
14. Joint Committee of Structural Safety. Probabilistic Model Code. 2001. Available online: http://www.jcss.byg.dtu.dk/Publications/Probabilistic_Model_Code.aspx (accessed on 4 January 2015).
15. Vencel, A.; Rac, A. Diesel engine crankshaft journal bearings failures: Case study. *Eng. Fail. Anal.* **2014**, *44*, 217–228.
16. Mehdizadeh, M.; Khodabakhshi, F. An investigation into failure analysis of interfering part of a steam turbine journal bearing. *Case Stud. Eng. Fail. Anal.* **2014**, *2*, 61–68.
17. He, Y.; Zhao, Z.; Luo, T.; Lu, X.; Luo, J. Failure analysis of journal bearing used in turboset of a power plant. *Mater. Des.* **2013**, *52*, 923–931.
18. Palmer, E.B. Aircraft wheel bearing failures...why? *Ind. Lubr. Tribol.* **1961**, *13*, 20–24.
19. Roeder, C.; Stanton, J.; Taylor, A. Fatigue of Steel-Reinforced Elastomeric Bearings. *J. Struct. Eng.* **1990**, *116*, 407–426.
20. Barden Precision Bearings—Bearing Failure: Causes and Cures. Available online: <http://www.bardenbearings.com/content.barden.us/en/services/mediathek/mediathek.jsp> (accessed on 5 January 2015).
21. The Timken Company—Timken Bearing Damage Analysis with Lubrication Reference Guide. Available online: <http://www.timken.com/> (accessed on 23 February 2015).
22. Sánchez, E.V.; Hansen, R.H.; Kramer, M. Control performance assessment and design of optimal control to harvest ocean energy. *IEEE J. Ocean Eng.* **2015**, *40*, 15–26.
23. Nambiar, A.J.; Forehand, D.I.M.; Kramer, M.; Hansen, R.H.; Ingram, D.M. Effects of hydrodynamic interactions and control within a point absorber array on electrical output. *Int. J. Mar. Energy* **2015**, *9*, 20–40.
24. Schaeffler—Product Selection Webpage. Available online: <http://medias.schaeffler.de/medias/en!hp/> (accessed on 4 January 2015).
25. Motion Industries—Product Catalog. Available online: <http://www.motionindustries.com> (accessed on 13 January 2015).
26. Ambühl, S.; Marquis, L.; Kofoed, J.P.; Sørensen, J.D. Operation and maintenance strategies for wave energy converters. *J. Risk Reliab.* **2015**, *229*, 417–441.
27. Smith, J.O.; Liu, C.K. Stresses due to tangential and normal loads on an elastic solid with application to some contact stress problems. *J. Appl. Mech.* **1953**, *20*, 157–166.
28. *ASTM Standard for Cycle Counting Fatigue Analysis*; ASTM Standard E 1049-1085; American Society for Testing and Materials (ASTM): West Conshohocken, PA, USA, 1995.
29. Xu, X.; Yu, Z. Failure analysis of GCr15SiMn steel bearing sleeve. *Eng. Fail. Anal.* **2006**, *13*, 857–865.
30. Li, W.; Sakai, T.; Li, Q.; Lu, L.T.; Wang, P. Reliability evaluation on very high cycle fatigue property of GCr15 bearing steel. *Int. J. Fatigue* **2010**, *10*, 1096–1107.
31. Pattabhiraman, S.; Levesque, G.; Kim, N.H.; Arakere, N.K. Uncertainty analysis for rolling contact fatigue failure probability of silicon nitride ball bearings. *Int. J. Solids Struct.* **2010**, *47*, 2543–2553.
32. *Guide to Methods for Assessing the Acceptability of Flaws in Metallic Structures*; British Standards (BS): London, UK, 2005.
33. Li, W.; Wang, P.; Lu, L.-T.; Sakai, T. Evaluation of gigacycle fatigue limit and life of high-strength steel with interior inclusion-induced failure. *Int. J. Damage Mech.* **2014**, *23*, 931–948.
34. *Safety Factors—Background Document*; IEC 61400-1-MT01; International Electrotechnical Commission (IEC): Geneva, Switzerland, 2013.
35. Sørensen, J.D. Reliability-based Calibration of fatigue safety factors for offshore wind turbines. In Proceedings of the 21st International Society of Offshore and Polar Engineers (ISOPE) Conference, Maui, HI, USA, 19–24 June 2011.
36. Sørensen, J.D.; Tarp-Johansen, N.J. Reliability-based optimization and optimal reliability level of offshore wind turbines. In Proceedings of the 15th International Society of Offshore and Polar Engineers (ISOPE) Conference: Seoul, South Korea, 19–24 June 2005.
37. The Engineering Toolbox. Friction and Coefficients of Friction. Available online: http://www.engineeringtoolbox.com/friction-coefficients-d_778.html (accessed on 11 February 2015).

38. Stephens, R.I.; Fatemi, A.; Stephens, R.R.; Fuchs, H.O. *Metal Fatigue in Engineering*, 2nd ed.; John Wiley & Sons, Inc.: New York, NY, USA, 2001.
39. FERUM: Finite Element Reliability Using Matlab. Available online: <http://www.ce.berkeley.edu/projects/ferum/> (accessed on 25 August 2014).



© 2016 by the authors; licensee MDPI, Basel, Switzerland. This article is an open access article distributed under the terms and conditions of the Creative Commons by Attribution (CC-BY) license (<http://creativecommons.org/licenses/by/4.0/>).